

The Atmospheric Signatures of Super-Earths: How to Distinguish Between Hydrogen-Rich and Hydrogen-Poor Atmospheres

Eliza Miller-Ricci

Harvard-Smithsonian Center for Astrophysics, 60 Garden St. Cambridge, MA 02138

`emillerricci@cfa.harvard.edu`

Sara Seager

*Department of Earth, Atmospheric, and Planetary Sciences, Department of Physics,
Massachusetts Institute of Technology, 54-1626, 77 Massachusetts Ave., Cambridge, MA 02139*

Dimitar Sasselov

Harvard-Smithsonian Center for Astrophysics, 60 Garden St. Cambridge, MA 02138

ABSTRACT

Extrasolar super-Earths ($1-10 M_{\oplus}$) are likely to exist with a wide range of atmospheres. Some super-Earths may be able to retain massive hydrogen-rich atmospheres. Others might never accumulate hydrogen or experience significant escape of lightweight elements, resulting in atmospheres more like those of the terrestrial planets in our Solar System. We examine how an observer could differentiate between hydrogen-rich and hydrogen-poor atmospheres by modeling super-Earth emission and transmission spectra, and we find that discrimination is possible by observing the transmission spectrum alone. An Earth-like atmosphere, composed of mostly heavy elements and molecules, will have a very weak transmission signal due to its small atmospheric scale height (since the scale height is inversely proportional to molecular weight). On the other hand, a large hydrogen-rich atmosphere reveals a relatively large transmission signal. The super Earth emission spectrum can additionally constrain the atmospheric composition and temperature structure. Super-Earths with massive hydrogen atmospheres will reveal strong spectral features due to water, whereas those that have lost most of their hydrogen (and have no liquid ocean) will be marked by CO_2 features and a lack of H_2O . We apply our study specifically to the low-mass planet orbiting an M star, Gl 581c ($M_{\text{sin}i} = 5 M_{\oplus}$), although our conclusions are relevant for super-Earths in general. The ability to distinguish hydrogen-rich atmospheres might be essential for interpreting mass and radius observations of planets in the transition between rocky super-Earths and Neptune-like planets.

Subject headings: stars: individual (Gl 581) - planetary systems

1. Introduction

The search for extrasolar planets has recently resulted in the discovery of a new class of planets, super-Earths, with masses between about 1 and 10 Earth masses (M_{\oplus}) (Rivera et al. 2005; Beaulieu et al. 2006; Udry et al. 2007). Since no such planets exist in our Solar System, the bulk composition of these planets and of their atmospheres remains largely unknown, although some theoretical work on the subject has been presented. In contrast to rocky planets in our Solar System, super-Earths are predicted to have large surface gravities, - upwards of 25 m/s^2 for a $5 M_{\text{earth}}$ planet - (Valencia et al. 2006, 2007; Fortney et al. 2007; Seager et al. 2007; Sotin et al. 2007) and some super-Earths may therefore be able to retain massive H-rich atmospheres. Others will bear a closer resemblance to Earth, with atmospheres depleted in hydrogen and composed of predominantly heavier molecules. A third interesting case is that some super-Earths may lie in between these two extremes, with moderate levels of atmospheric hydrogen due to either incomplete escape of hydrogen over the planet’s lifetime and/or from outgassing of a significant secondary H_2 atmosphere. The question arises as to whether these cases will differ in their gross observable properties, and how. In the interest of discovering habitable planets and learning more about atmospheric evolution on super-Earths, it will be necessary to find a method for discriminating between the possible types of atmospheres. This issue has led us to model the observational signature for the various possible atmospheres on the low-mass planet, Gl 581c (Udry et al. 2007).

The bulk composition of planets in the mass range between Earth and Neptune carries important clues to understanding planet formation. Even the simple statistical distribution of very water-rich versus dry super-Earths in an observed sample would be sufficient (Valencia et al. 2007). Unfortunately, with planet mass and radius alone the internal structure models have degeneracies, which become almost untractable when a hydrogen-rich envelope covers the planet (Adams et al. 2008). Our study in this paper points to a potential solution to breaking this degeneracy, by distinguishing a hydrogen-rich atmosphere spectroscopically.

A number of observations of transiting hot Jupiters have already allowed for constraints to be placed on the nature of their atmospheres. IR observations of the secondary eclipse (when the planet passes behind its host star) have resulted in measurements of brightness temperatures (Deming et al. 2005; Charbonneau et al. 2005; Deming et al. 2006; Harrington et al. 2007; Deming et al. 2007; Demory et al. 2007; Knutson et al. 2008) as well as emission spectra (Grillmair et al. 2007; Richardson et al. 2007; Swain et al. 2007; Charbonneau et al. 2008) for several hot Jupiters. Optical transmission spectra for HD 209458b have led to the discovery of several species in the planet’s atmosphere including sodium (Charbonneau et al. 2002), hydrogen (Vidal-Madjar et al. 2003; Ehrenreich et al. 2008), and tentative detections of oxygen and carbon (Vidal-Madjar et al. 2004). Recent observations of the IR transmission spectrum of HD 189733b have led to the first discoveries of water (Tinetti et al. 2007; Beaulieu et al. 2008) and methane (Swain et al. 2008) in the atmosphere of an extrasolar planet. Additionally, attempted observations of the optical secondary eclipse of HD 209458b using the *MOST* space telescope have allowed for strong limits to be placed on the planet’s optical albedo (Rowe et al. 2006, 2007). Since super-Earths are smaller

than hot Jupiters, these types of measurements will prove more challenging for this new class of planets (Seager et al. 2008). However, it will most likely be these same types of observations that will eventually aid in characterizing the atmospheres of low-mass planets.

The discovery of the low-mass planet Gl 581c ($M_{\text{sin}} = 5M_{\oplus}$) has generated a large amount of interest in the literature, and a number of authors have already explored the question of habitability for this planet after an initial claim by Udry et al. (2007) that Gl 581c may reside inside its star’s habitable zone. It now appears that the planet is probably too hot to host liquid water unless its surface is mostly obscured by highly reflective clouds (Selsis et al. 2007), or the planet is tidally locked, with the night side receiving sufficient heat circulation from the day side of the planet (Chylek & Perez 2007). To further confirm this conclusion, von Bloh et al. (2007b,a) have examined the possibility of sustained photosynthetic life on Gl 581c and have ruled this out on the grounds that the planet cannot keep sufficient CO_2 in its atmosphere for photosynthesis to occur, while at the same time retaining a surface temperature cool enough for liquid water. However, in terms of climate stability, Beust et al. (2007) have modeled the dynamic evolution of the Gl 581 system. They find that the orbit (and therefore the climate) of Gl 581c should be secularly stable over 10^8 yrs, leaving open a possibility that life of a more exotic variety could still develop on this planet.

In this paper, we address a different question relating to the nature of Gl 581c’s atmosphere. What observations are needed to constrain the atmospheric composition and overall hydrogen content for Gl 581c or similar super-Earths? To this end, we investigate several scenarios for the composition of the super-Earth atmosphere ranging from hydrogen-rich to hydrogen-poor. The cases that we explore are (i) a massive hydrogen-rich (reducing) atmosphere obtained through accretion of nebular gas, (ii) a mildly reducing atmosphere that has lost most but not all of its hydrogen due to atmospheric escape processes, and (iii) an oxidizing CO_2 -rich atmosphere similar in composition to that of Venus that contains essentially no hydrogen. From the modeled spectra, we determine how to observationally differentiate between the various scenarios. We describe our model atmosphere in § 2 and our three scenarios for atmospheric composition in § 3. In § 4 we reveal the modeled emission and transmission spectra for Gl 581c, and we determine how hydrogen content can be established through observations. Finally, we summarize our results and discuss their implications in § 5.

2. Super Earth Atmosphere Model

2.1. Opacities

We determine molecular opacities following the procedure outlined in Seager et al. (2000) for wavelengths ranging from 0.1 to 100 μm . We include the dominant sources of molecular line opacity in the IR: CH_4 , CO , NH_3 , (Freedman et al. 2007, and references therein), H_2O (Freedman et al. 2007; Partridge & Schwenke 1997), CO_2 , O_2 , and O_3 (Rothman et al. 2005). CO_2 - CO_2 collision induced opacities are also included (Brodbeck et al. 1991), which we find to have an effect on

the near-IR portion of some of the super-Earth spectra. We have not included opacities of any condensed species including the solid and liquid forms of water, since we find that none of our atmospheres enter into the temperature and pressure regime of water clouds.

2.2. Chemistry

Given the atomic makeup of our super-Earth atmosphere, we determine molecular abundances in chemical equilibrium. This is accomplished by minimizing Gibbs free energy following the method outlined in White et al. (1958) for 23 atoms and 172 gas phase molecules. For the Gibbs free energies of each molecule we use polynomial fits from Sharp & Huebner (1990), which we find to be a good match to data from the NIST JANAF thermochemical tables (Chase 1998) over our full temperature range of interest (100-1000 K). We do not include a full treatment of condensed species in our chemical model, although we do determine whether any of our model atmospheres cross the condensation curves of known cloud-forming species. Specifically, we look for condensation of H_2O and stability of the H_2SO_4 condensate, since both are known to form clouds on planets of the inner Solar System and could potentially alter the T-P profile and planetary emission spectrum predicted by our models.

We find that chemical equilibrium for a super-Earth atmosphere containing large quantities of hydrogen predicts high abundances of both ammonia and methane. However, these two species are known to be destroyed readily by UV photolysis in planetary atmospheres. Determining NH_3 and CH_4 abundances in photochemical equilibrium would involve knowledge of the full range of chemical reactions that take place in the super-Earth atmosphere and their reaction rates as a function of temperature. Compiling such a model for the range of atmospheric chemistries that we consider for Gl 581c is beyond the scope of this paper. Instead, we calculate photolysis lifetimes for both NH_3 and CH_4 , and we assume that return reactions replenishing these molecules occur slowly, which is generally correct in the temperature range that we consider. Molecules are then determined to be photochemically unstable if their photolysis lifetimes, $1/J(z)$, are found to be less than the age of the planet (approximately 4.3 Gyr (Udry et al. 2007)) throughout a significant portion of the atmosphere. Since atmospheric overturning timescales should be short - on the order of hours (Massie & Hunten 1981) - mixing will occur readily to regions where the molecules are destroyed by photolysis. Here $J(z)$ is the photodissociation rate at height z in the atmosphere:

$$J(z) = \int \sigma_\nu F_\nu e^{-\tau_\nu} d\nu, \quad (1)$$

where σ_ν is the photodissociation cross-section at frequency ν and F_ν is the incident solar flux expressed in photons $\text{cm}^{-2} \text{s}^{-1} \text{Hz}^{-1}$. The optical depth, τ_ν is given by

$$\tau_\nu(z) = \int_z^{z_{max}} \kappa_\nu ds, \quad (2)$$

where κ is the opacity in units of cm^{-1} . Here we have included contributions both from absorption of photons and from Rayleigh scattering, which can have a significant effect in shielding the atmosphere

from UV penetration at the shortest wavelengths. We obtain UV cross-sections for the major constituents of the atmosphere from Yung & Demore (1999). The UV flux from Gl 581 is taken from IUE observations as reported by Buccino et al. (2007) and scaled to a distance of 0.073 A. U.

If methane and ammonia are found to be sufficiently short-lived, we then remove these species from our chemical model. In practice this is accomplished by recalculating chemical equilibrium without the presence of NH_3 and CH_4 . Their atomic constituents are then reallocated to the most stable molecules - N_2 and H_2 in the case of ammonia, and H_2 , CO , and CO_2 for methane. The resulting chemical compositions for the Super-Earth atmospheres that we consider are presented in Section 3.

2.3. Irradiated Temperature-Pressure Profile

We compute a 1-D radial radiative-convective temperature-pressure (T-P) profile for Gl 581c. We have taken a fairly basic approach toward generating the T-P profile in that we assume a grey atmosphere in hydrostatic equilibrium. However, we point out that the major results we present later in this paper for transmission spectra are not strongly dependent on the exact T-P profile that is used.

For the temperature structure, we make the assumption of an irradiated grey atmosphere as presented by Chevallier et al. (2007) and Hansen (2007). The planet’s temperature profile as a function of optical depth τ is described by

$$T^4 = \frac{3}{4}T_{eff}^4 \left[\tau + \frac{2}{3} \right] + \mu_0 T_{eq}^4 \left[1 + \frac{3}{2} \left(\frac{\mu_0}{\gamma} \right)^2 - \frac{3}{2} \left(\frac{\mu_0}{\gamma} \right)^3 \ln \left(1 + \frac{\gamma}{\mu_0} \right) - \frac{3}{4} \frac{\mu_0}{\gamma} e^{-\gamma\tau/\mu_0} \right]. \quad (3)$$

Here μ_0 is the cosine of the angle between each point on the planet’s surface and the illuminating star; T_{eq} is the planet’s equilibrium temperature; T_{eff} describes the additional contribution due to internal heating such that $T^4 = T_{eff}^4 + T_{eq}^4$ at optical depth $2/3$ and $\mu_0 = 1$; and γ is the ratio of the optical depth of absorption to that of emitted radiation, which parameterizes the deposition of stellar energy into the planetary atmosphere. A self-consistent value for the factor γ is determined iteratively after computing the emission and transmission spectra of the planet (Section 2.5). Our choices for the other model inputs to Eq. 3 are as follows. Since we do not model the scattering properties of the planetary atmosphere, we must assume values for the planet’s albedo and its implied T_{eq} . We employ an albedo of 0.15 for cloud-free models and 0.65 for models with sulfuric acid clouds, resulting in values of $T_{eq} = 368$ K and 295 K respectively. Despite the presence of additional planets in the Gl 581 system, tidal heating due to these bodies should not add significantly to the planet’s observed temperature (Wade Henning, private communication), and other sources internal heating should be small. However, our temperature model requires that a small but non-zero value be employed for the internal heating via the parameter T_{eff} , to ensure a physically realistic temperature profile at high optical depths. We choose a value of $T_{eff} = 50$ K, which adds negligibly to the global energy emitted by the planet at optical depth of unity.

The pressure structure of our super-Earth atmosphere is calculated by integration of the equation of hydrostatic equilibrium

$$\frac{dP}{d\tau} = \frac{g}{\kappa_{gr}}, \quad (4)$$

where κ_{gr} is the Planck mean opacity in units of cm^2/g .

We check the resulting radiative temperature-pressure profile for instability to convection according to the stability criterion

$$\frac{d\ln T}{d\ln P} < \nabla_{ad}, \quad (5)$$

where $\nabla_{ad} = (\gamma - 1)/\gamma$, and γ is the adiabatic index. If this criterion is satisfied then we employ the radiative T-P profile described above. Otherwise, we assume that the atmospheric T-P profile follows an adiabat with the appropriate lapse rate. The resulting temperature-pressure profiles for the atmospheres described in the following section are shown in Figure 1 along with those of Venus and Earth as a reference.

2.4. Atmospheric Mass

The mass of the Gl 581c’s atmosphere is one of the major unknowns involved in any model. In our own Solar System, the atmospheric masses of similarly-sized Earth and Venus vary by almost two orders of magnitude, which implies that other factors such as formation history or the presence of liquid oceans have a large effect. Fortunately, the results we present in this paper have little dependence on the mass of the atmosphere (see Section 4).

For our models, we pick an atmospheric mass and then ensure consistency with our chosen optical depth scale. We determine the atmospheric density, $\rho(r)$, as a function of height, given our T-P profile and the chemistry that is implied, using an ideal gas equation of state. The total mass contained in the atmosphere, M_{atm} , is then calculated by integrating the equation of conservation of mass upward from the planet’s surface through the atmosphere

$$M_{atm} = \int 4\pi r^2 \rho(r) dr, \quad (6)$$

where r is the distance from the planet’s center. Given the atmospheric mass that we have decided upon for a given model, we iteratively adjust the value for τ at the base of the atmosphere until our calculated atmospheric mass agrees with the value of the model input. In Section 3 we discuss our choices of mass for the different atmosphere scenarios.

2.5. Emission and Transmission Spectra

To determine the planet’s emitted spectrum, we integrate the equation of radiative transfer through the planet’s atmosphere. Using the T-P profile as outlined in Section 2.3, we obtain the

emergent intensity, I , by

$$I(\lambda, \mu) = \frac{1}{\mu} \int_0^\tau S(T) e^{-\tau'/\mu} d\tau', \quad (7)$$

where S is the source function, μ is the cosine of the viewing angle, and τ is the optical depth at the base of the atmosphere. We have made the simplifying assumption of a Planckian source function. We also do not consider scattering, which is a valid assumption in the IR where this is generally a small effect. We have tested the validity of both of these assumptions by using this scheme to reproduce Earth and Venus’ emitted spectra, given their known T-P profiles. We simulate Venus’ opaque H_2SO_4 cloud deck by cutting off the planetary emission at an altitude of 70 km above the surface. Our resulting spectra are in agreement with the expected planet-averaged emission for both of these cases (Moroz et al. 1986; Hanel et al. 1972).

If the planet’s orbit is aligned such that it transits its host star, then the atmospheric transmission spectrum can potentially be observed. During transit, light from the star passes through the optically thin upper layers of the planet’s atmosphere, leading to excess absorption of star light at certain wavelengths. We compute theoretical transmission spectra by determining the amount of absorption from light rays passing through the planet’s atmosphere, along the observer’s line of sight. The geometry we employ is similar to the one presented in Ehrenreich et al. (2006, their Figure 1), where the solid core of the planet is represented by an optically thick disk of radius $1.4 R_\oplus$. We calculate transmission through the annulus of gas surrounding this disk, which represents the planet’s atmosphere. The resultant intensities are then given by the expression

$$I(\lambda, \mu) = I_0 e^{-\tau/\mu}, \quad (8)$$

where I_0 is the incident intensity from the star and τ is now the slant optical depth integrated through the planet’s atmosphere along the observer’s line of sight. We once again only include absorption here and do not include the effects of additional scattering out of the beam, which we find to have a negligible effect longward of $1 \mu\text{m}$. We then integrate over the entire annulus of the atmosphere to determine the total excess absorption of stellar flux as a function of wavelength.

To calculate transmission spectra, it is necessary to assume a planetary radius, R_p . This is required both to determine the amount of stellar flux that is blocked out during transit as well as for computing path lengths through the planet’s atmosphere. Since there are no transit observations available for Gl 581c, R_p becomes a free parameter in our model. We therefore rely on theoretical predictions of the mass-radius relationship for super-Earths and choose a radius of $1.4 R_\oplus$, corresponding to a rocky planet with a composition similar to Earth, composed of 67.5% silicate mantle and 32.5% iron core (Seager et al. 2007; Valencia et al. 2007).

3. Atmospheric Composition

The formation history of Gl 581c is largely unknown, and similarly, the mechanism by which the planet obtained its atmosphere remains uncertain. In particular, for the terrestrial planets in

our Solar System, the issue of atmospheric escape plays a central role in our understanding of these planets’ histories. Since estimates of atmospheric escape rates for hot giant exoplanets are uncertain to several orders of magnitude (Baraffe et al. 2004; Hubbard et al. 2007), it is not clear whether Gl 581c and similarly sized Super-Earths would be able to retain large amounts of molecular hydrogen in their atmospheres.

In the thermal limit, the ability of an atmosphere to retain hydrogen is described by the escape parameter

$$\lambda = \frac{R_{pl}}{H}, \quad (9)$$

where H is the atmospheric scale height for hydrogen at the exobase. The factor λ is also equivalent to the square of the ratio between the escape speed and mean thermal speed of the gas. High values of λ ($\gtrsim 15$) mean that the atmosphere will be retained, while planets with low values will experience atmospheric escape. For reference, in Earth’s atmosphere λ is between 5 and 10 for hydrogen. For Gl 581c, the planet’s high escape speed potentially implies an escape parameter larger than 15. However, our atmosphere model does not include the UV information necessary to predict exobase temperatures, and at present the XUV flux from Gl 581 is unconstrained.

From this argument, thermal escape of atomic hydrogen of Gl 581c may be unlikely. However, a variety of nonthermal escape processes can procede at much faster rates than thermal escape. These are known to dominate in many cases (Hunten et al. 1989) and are more difficult to constrain. Gl 581c therefore lies in a region of parameter space where it is unclear whether the planet is able to retain hydrogen over its lifetime. As a further complication, the initial amount of outgassing of hydrogen and other gasses from the planetary surface is almost entirely unconstrained, making it difficult to ascertain how hydrogen loss would contribute to the present atmospheric composition (Elkins-Tanton & Seager 2008).

Since the amount of atmospheric hydrogen is therefore poorly constrained, and in order to present results of more general relevance, we choose to model three distinctly different atmospheres for Gl 581c. These vary in their composition and in the ways by which they would be acquired by the planet. The three cases that we choose also span the range from hydrogen-rich to hydrogen-poor in our effort to understand the different observational signatures of these types of atmospheres. The scenarios are outlined as follows.

3.1. Hydrogen-Rich Atmosphere

Our first model atmosphere represents one obtained through a standard accretion process that experiences little evolution later in its lifetime. In this scenario, after formation of a solid core, Gl 581c would accrete its atmosphere through gravitational capture of gas from the protoplanetary disk, resulting in a composition that more or less reflects that of the stellar nebula. It is assumed that this atmosphere is sufficiently massive and experiences low escape rates, such that the planet

is able to retain large quantities of hydrogen. This results in a reducing chemistry where hydrogen-bearing molecules dominate the atmosphere.

To calculate the detailed composition for the atmosphere of Gl 581c we use the observed architecture of the Gl 581 planet system to infer that all three Gl 581 planets formed at about 2-5 times larger orbital radii and migrated to their current locations. This would imply that both Gl 581c and d had access to volatiles during formation beyond the snow line, similarly to the HD 69830 system with three Neptunes described in Lovis et al. (2006). For HD 69830 Beichman et al. (2005) have done IR spectroscopy of the debris disk between the orbits of HD 69830c and d, finding a volatile mix corresponding to a disk producing cometary body like Hale-Bopp, with its known bulk composition (Irvine et al. 2000). By analogy, we assume the same bulk composition for Gl 581c, or any super-Earth planet under similar conditions. This calculation results in an atmosphere of Gl 581c that is composed by mass of 73.2% H, 22.6% He, 3.5% C, N, and O, 0.2% Ne, and 0.5% other heavy elements appearing in solar composition ratios (see Table 1). To determine the resulting molecular composition of the atmosphere we apply the conditions of chemical equilibrium as discussed in Section 2.2. The resulting mixing ratios for the major constituents of this atmosphere are shown in the top panel of Figure 2 (solid lines).

Due to its large hydrogen content, the chemical equilibrium calculation requires that this atmosphere have high abundances of hydrogen-bearing molecules such as H_2 , H_2O , CH_4 , and NH_3 . However, as mentioned in Section 2.2, ammonia and methane are apt to be destroyed by UV radiation from the star. We determine the photochemical lifetimes of NH_3 and CH_4 as a function of height above the planet’s surface according to Eq. 1, and we determine that UV photodissociation should readily remove ammonia and methane from the atmosphere as long as any chemical reactions that create these molecules occur slowly. We therefore include a photochemical model for the hydrogen-rich scenario, where NH_3 and CH_4 are completely removed from the atmosphere along with the chemical equilibrium model, as shown in Figure 2.

We employ an atmospheric mass for this model that is scaled up by a factor of 4 compared to that of the Earth, to account for the large quantity of hydrogen that remains in this atmosphere. However, this number remains somewhat arbitrary since the true mass of the atmosphere for this scenario is dependent on the amount of gas that can be gravitationally captured and then retained by a planet of this size. Our choice of atmospheric mass has indirect implications for photochemistry as well in that a more massive atmosphere may have some remaining CH_4 and NH_3 present if these species are only readily destroyed in the upper atmosphere.

3.2. Intermediate Hydrogen Content Atmosphere

Our second case falls midway between a hydrogen-rich atmosphere and one that has lost all of its hydrogen through escape processes. We work under the assumption here that Gl 581c has experienced atmospheric evolution to the point that it has lost a large amount of the hydrogen

obtained in the accretion process. However, in this scenario, the atmosphere has still managed to retain some hydrogen so that the atmospheric chemistry remains mildly reducing. This type of atmospheric chemistry does not occur in any Solar System bodies, however it is possible that such an atmosphere could take hold on Gl 581c via a number of methods. One possibility is that atmospheric escape occurred early on in the planet’s life when Gl 581 was still in a young active phase, but that the escape process was cut off prematurely as the M-star evolved and produced a reduced UV and X-ray flux. This is similar to what is known to occur in solar-type stars as they age, where UV flux reduces by a factor of 10^3 over their main-sequence lifetimes (Ribas et al. 2005). A second possibility is that the planet did lose its entire atmosphere early on in its history through hydrodynamic escape, and that this represents a secondary atmosphere obtained through planetary outgassing. Large quantities of H_2 can potentially be outgassed through the process $H_2O + Fe \rightarrow FeO + H_2$ (Elkins-Tanton & Seager 2008), and much of this hydrogen may be retained due to the high surface gravity of the super-Earth.

We choose to work under the first assumption that Gl 581c has experienced incomplete loss of its atmospheric hydrogen. The outgassing scenario is viable as well, although it is difficult to predict what the resulting atmospheric composition would resemble without a more complete picture of the interior composition and formation history of the planet. We therefore assume that Gl 581c is not an ocean planet and that the lightest constituents of the atmosphere have been able to escape during the lifetime of the planet. Our evaporated case then develops in the direction of Mars’ atmosphere with He and Ne becoming trace constituents. The atmospheric hydrogen would mostly escape as well, and what remains is locked in heavier molecular species (mostly H_2O and CH_4).

To determine the atmospheric composition for this scenario, we start with the hydrogen-rich atmosphere described above and then assume that a portion of the hydrogen is allowed to escape to the point that it is reduced to half of its initial abundance. With what remains we then recalculate chemical equilibrium to determine the resultant composition of the atmosphere. This process results in an atmosphere that has experienced a partial loss of hydrogen, but still leaves behind a reduced but non-negligible amount of molecular hydrogen in the planet’s atmosphere (about 1-10% by volume). The rest of the atmosphere is made up mostly of water vapor, CO_2 , CH_4 , and N_2 . Photochemistry once again affects the upper atmosphere in this scenario in that methane and ammonia are photochemically unstable. We therefore remove these two molecules from our model, and we present this case along with the case of chemical equilibrium in Figure 2 (middle panel). For this scenario we have chosen an atmospheric mass equivalent to that of Earth’s atmosphere.

3.3. Hydrogen-Poor Atmosphere

For our final scenario, we examine what the atmosphere of Gl 581c would resemble if it had a similar formation history to those of the terrestrial planets in our Solar System. We choose a composition mirroring that of Venus’ atmosphere, where it is assumed that there has been an almost complete loss of hydrogen through molecular photodissociation and subsequent escape. For

Venus, the planetary surface is too warm for liquid H_2O , and carbon remains free in the atmosphere rather than being sequestered to the bottom of a water ocean. This is most likely the case for Gl 581c as well, since the planet is expected to have a high surface temperature (Selsis et al. 2007). The oxidizing nature of this atmospheric chemistry then leads to the formation of large quantities of CO_2 , which becomes the primary source of opacity. To keep with the comparison to Venus, we have also given this atmosphere a mass equal to Venus’ atmospheric mass, or about 100 times greater than that of the Earth. We assume that this planetary atmosphere has the same atomic makeup as Venus (Table 1), and the resulting equilibrium molecular composition as a function of height is shown in Figure 2.

For a Venusian atmosphere, photochemistry plays a role in aiding in the formation of sulfuric acid clouds via the reaction $2\text{SO}_2 + \text{O}_2 + 2\text{H}_2\text{O} \rightarrow 2\text{H}_2\text{SO}_4$. As long as the planet’s atmosphere contains some SO_2 this process will occur, and under the right conditions this will result in a cloud layer on Gl 581c just like the one on Venus. Super-Earths, being more massive than Venus, are very likely to outgas larger amounts of SO_2 and H_2S than Venus did. With loss of H in this scenario, the concentration of SO_2 will be larger than what it is in Venus. About 50% of the sulfur will be outgassed as H_2S (Wallace & Carmichael 1994). For sulfuric acid clouds to exist on Gl 581c, the partial pressure of H_2SO_4 must be sufficiently large such that its temperature-pressure curve in the atmosphere crosses the condensation curve. For this scenario, condensation will then occur if the abundance of sulfuric acid exceeds 0.5 parts per million (ppm). For reference, on Venus the H_2SO_4 abundance just below the cloud deck is approximately 10 ppm. For Gl 581c, sulfuric acid abundances ranging from 3 ppm to 0.3% will result in clouds ranging in location from $P = 0.15$ bar ($T = 400$ K) to 25 km $P = 25$ mbar ($T = 300$ K) above the planet’s surface. Due to the uncertainties in this cloud model, in the following sections we present models both with and without sulfuric acid clouds for the hydrogen-poor scenario.

4. Results

4.1. Transmission Spectra as a Probe of Hydrogen Content

Our most significant finding is that transmission spectra are the best method for distinguishing between hydrogen-dominated atmospheres and hydrogen-poor atmospheres. For a conceptual explanation, we can consider an exoplanet atmosphere to have a vertical extent of $10 H$, where H is the scale height,

$$H = \frac{kT}{\mu_m g}. \quad (10)$$

The scale height, is proportional to the inverse of the atmospheric mean molecular weight μ_m , expressed from here on in terms of atomic mass units (u). In hydrogen-dominated atmospheres, $\mu_m \simeq 2$, and H is large. In contrast, in our hydrogen-poor atmosphere, $\mu_m \simeq 40$, making the scale height, and hence the atmosphere available for transmission, less by a factor of 20. Measuring the change in eclipse depth ΔD across spectral lines in transmission gives an order of magnitude

approximation of the scale height according to

$$\Delta D \sim \frac{2HR_{pl}}{R_*^2}, \quad (11)$$

allowing for a determination of μ_m assuming that both the atmospheric temperature and surface gravity are known to within a factor of a few. This will indeed be the case as long as we assume that the equilibrium temperature of the planet predicts its actual temperature to within a factor of several and that the radius and mass of the planet are known, allowing for a calculation of g . Measurement of the scale height should therefore offer a strong constraint on the atmospheric composition in terms of its hydrogen content, via the parameter μ_m , even if the exact T-P profile of the atmosphere is unknown. This interplay between scale height and transmission signal has also been pointed out by Ehrenreich et al. (2006) for low-mass transiting planets.

The sensitivity of scale height to atmospheric composition is illustrated in Figure 3, where we show scale height as a function of effective temperature for a variety of different μ_m . The implication is that, for the same mass of atmosphere, one that is made predominantly of hydrogen will tend to be larger and therefore more readily observable in transmission. For the other two cases where the atmosphere is composed predominantly of heavier molecules, we have the opposite case. Additionally, since scale height drops off as T_{eff} decreases, planets that are farther away from their host stars (and hence colder) will also be difficult to observe in transmission. This has implications for follow-up of transiting giant planets discovered by the Kepler (Borucki et al. 2004; Basri et al. 2005) mission, since they will detect planets with orbital periods of a year or more.

In Figure 4 we have plotted our modeled spectra for each of the three cases of atmospheric composition that were discussed in Section 3. As expected from the scale height argument presented above, the hydrogen-rich atmosphere shows deep absorption features in transmission at a level of up to 10^{-4} . The other two atmospheres have weaker features – by about a factor of 10 for the intermediate atmosphere, and even weaker for the hydrogen-poor atmosphere. In the latter cases, due to the small scale height, the transmission spectrum only probes a very narrow range of height in the atmosphere. This result holds true independently of the T-P profile that we employ.

Ideally, with the capability to detect transmission spectra at a level of less than a part in 10^{-5} relative to the star, we could learn about the hydrogen content of a super-Earth atmosphere like Gl 581c. IR transmission spectroscopy would be the easiest way to differentiate between the various atmospheric cases, however narrow-band photometry from Spitzer is currently the best that can be accomplished. In Figure 4 we also show the expected relative fluxes in each of the Spitzer IRAC bands and in the MIPS 24- μm band for each model atmosphere. Each of the Spitzer bands averages over a number of spectral features, which effectively smooths out much of the transmission signal. However there are perceptible changes from one channel to the next that could be suggestive of atmospheric composition and hydrogen content. In the case of the hydrogen-rich atmosphere, the expected Spitzer IRAC fluxes vary from band to band at a level of 10^{-5} , while in the intermediate and hydrogen-poor cases this is reduced to a factor of 10^{-6} . For other exoplanet systems the expected transmission signal will vary according to Eq. 11. If photometry at this level can be

obtained, which will most likely need to wait for the launch of JWST, it will give observers a chance to place meaningful constraints on the atmospheric composition of super-Earths like Gl 581c.

Changing the atmospheric mass does little to alter the result presented above. In general, increasing the mass of the atmosphere serves to raise the height above the planet’s surface at which the atmosphere becomes optically thick. Since one can only see through optically thin layers, the result will be an overall transit radius that appears larger. This can be seen in Figure 4, where the hydrogen-rich atmosphere is the most massive one that we considered, and its transit radius appears somewhat larger than for the other cases by a factor of a few parts in 10^{-5} . However, the scale height itself, measured from the relative depth of the spectral lines, has very little dependence on atmospheric mass unless either chemistry or temperature changes dramatically as a function of height through the atmosphere. In summary, the depth of any spectral features observed in transmission should remain mostly independent of the atmosphere’s mass, and should depend most strongly on the scale height, H . This is an encouraging result, since the total mass of an atmosphere cannot be known a priori, and the values that we have assigned for atmospheric mass in this paper have been somewhat arbitrarily scaled from terrestrial planets in our Solar System. A negative corollary however, is that the mass of the atmosphere generally cannot be determined from the planet’s transmission spectrum.

4.2. Thermal Emission Spectrum

The planetary emission spectrum can also be generally helpful in discerning the chemistry and composition of a Super-Earth atmosphere. We find that the three types of atmosphere that we explored for Gl 581c each reveal very different emission spectra. The observed features in a planet’s emission spectrum represent the dominant sources of opacity in that atmosphere - H_2O for our hydrogen-dominated atmosphere, CO_2 for the hydrogen-poor atmosphere, and a combination of both in the intermediate hydrogen content case. The spectral features are therefore a strong indicator of the chemistry at work in the planetary atmosphere. Figure 5 shows the wavelength-dependent emission calculated for each of the three cases of atmospheric composition that we have explored. We have indicated the effect of methane and ammonia photochemistry on the emission spectra for the hydrogen-rich and intermediate cases, and the effect of a possible sulfuric acid cloud layer in the hydrogen-poor case.

In the hydrogen-rich case, atmospheric absorption lines are almost exclusively due to water. While methane and ammonia are not expected to be photochemically stable in this atmosphere, their outstanding presence would affect the emission spectrum between 5 and 15 μm . Suppression of flux in the 7 to 9 μm range is indicative of methane, and a strong feature between 10 and 11 microns could indicate the presence of ammonia.

The intermediate atmosphere with its mildly reducing chemistry exhibits strong features due

to both water and CO₂ absorption. The effect of ammonia photochemistry on this spectrum is minimal, while the presence or absence of methane can have a much larger impact. A complete loss of methane from this atmosphere results in a small spectral window from 2 to 3 μm where there is little to no opacity, and the atmosphere remains optically thin down to the planet’s surface. However, flux in this range can be further suppressed due to the presence of aerosols in the atmosphere, or by a lower surface temperature than the one employed in our model.

For the hydrogen-poor atmosphere the presence of clouds has a strong effect on the emission spectrum between 1 and 9 μm . In this scenario CO₂ is the predominant source of opacity, resulting in absorption features at 4.5 μm , 11 μm , and 15 μm . Weak water features are also present at longer wavelengths despite the low abundance of H₂O in this atmosphere. In the absence of clouds, there are few absorption features in the 1-8 μm range, and the atmosphere remains optically thin almost down to the planet’s hot surface. However, the presence of opaque clouds can greatly suppress the flux in this spectral range. Additionally, other sources of opacity between 1 and 8 μm that have not been accounted for in our model such as aerosols or photochemical hazes could suppress the emitted flux in this spectral range. For the cloudy hydrogen-poor model, we have placed an opaque cloud deck at a temperature of 400 K ($P = 200$ mbar). Moving this to higher in the atmosphere would result in an even lower emitted flux in the near-IR due to the lower temperatures in this region of the atmosphere.

To date, emission from extrasolar planets has been best measured through observations of secondary eclipses for transiting systems (when the planet passes behind its host star). The depth D of secondary eclipse can be expressed as

$$D = \frac{F_{pl}}{F_* + F_{pl}} \quad (12)$$

where F_{pl} and F_* are the planetary and stellar fluxes respectively. In Figure 6 we plot the secondary eclipse depths for our three model atmospheres in the 1-30 μm range. For the stellar spectrum we use a Kurucz model¹ with stellar parameters $T_{eff} = 3500$ K, $\log g = 5.0$, and $[\text{Fe}/\text{H}] = -0.3$. The three very differently shaped emission spectra for our atmosphere scenarios also manifest themselves in differing secondary eclipse depths, where the same spectral features from the planetary emission spectra in Figure 5 can be seen in Figure 6 as well. The expected eclipse depths for Gl 581c in the IR are all predicted to be less than 70 ppm with the exception of the cloud-free hydrogen-poor model.

In Figure 6 we also show the secondary eclipse depths for our three model atmospheres in each of the Spitzer IRAC bands and in the MIPS 24 μm band. The IRAC bands give good coverage of water features in both the hydrogen-rich and intermediate atmospheres, although the expected eclipse depths are quite small at less than 10 ppm. For the cloud-free hydrogen-poor atmosphere we predict large variations in eclipse depth between the IRAC channels, indicating the presence of

¹See <http://kurucz.harvard.edu/grids.html>

CO₂. However, for the cloudy hydrogen-poor model, features in this spectral range are washed out, and the IRAC bands simply sample the blackbody curve at the temperature of the top of the cloud deck. In terms of constraining the nature of the planet’s atmosphere, the detection of water features in the 1 - 10 μm range and the CO₂ feature in the 12-19 μm range would be highly indicative of the atmospheric chemistry at work. Additionally, detection of other hydrogen-bearing molecules such as CH₄ and NH₃ would be of interest as they point to the type of photochemical processes taking place in the planet’s atmosphere. Already methane has been detected in the atmosphere of a giant exoplanet at levels that are not easily explained with current models (Swain et al. 2008). Unfortunately, with the exception of the cloud-free hydrogen-poor model, detecting spectral features from secondary eclipse observations would necessitate observations with a precision of better than 10^{-5} , which is not yet feasible with current instruments. This factor becomes larger or smaller depending on the stellar and planetary radii and temperatures, since warmer planets and larger planets such as ocean planets are easier to detect. Additionally, Spitzer does not carry any instruments that are capable of broad band photometry between 10 and 20 μm , which effectively means that the telescope misses the large CO₂ feature at 15 μm . The types of measurements suggested by Figure 6 will therefore most likely need to await future instruments such as MIRI (Wright et al. 2003) aboard JWST.

Temperature inversions, where the atmospheric temperature *increases* as a function of height, have the potential to greatly alter the emission spectrum. However, the locations of the various spectral features (in terms of wavelength) are robust regardless of the temperature gradient and will therefore remain good indicators of atmospheric chemistry. In general, a temperature inversion at the right height in the atmosphere will result in a spectrum of emission lines rather than the absorption features presented in Figures 6 and 5. Spectra for atmospheres with inverted temperature profiles will therefore look quite different from the ones presented here, and for this reason emission spectra are also a strong indicator of the atmospheric temperature gradient.

Atmospheric mass can have a stronger effect on emission spectra than on transmission, although once again the effect is secondary. A larger atmospheric mass will result in a higher surface temperature, since the density of gas at the base of the atmosphere is greater. In the optically thin regime, a higher surface temperature translates to a larger overall continuum flux, so a more massive atmosphere could result in an emission signature that is easier to observe. Additionally, increasing the mass of the planet’s atmosphere can cause a shift from the optically thin to optically thick regime, which in turn can significantly alter the appearance of its emitted spectrum. This would apply more strongly to the visible portion of the spectrum however, since the atmosphere tends to be mostly optically thick in the IR. Additionally, if the changes in surface temperature and pressure between a massive atmosphere and a low-mass one are large enough to alter the atmospheric chemistry, then the absorption features in the emission spectrum will have a mass dependence as well. In terms of photochemistry, a more massive atmosphere has a higher likelihood of containing stable quantities of methane and possibly ammonia, which affects the emission spectrum as seen in Figure 5.

5. Discussion

We have determined a method for differentiating between Super-Earths with large hydrogen-rich atmospheres and those with atmospheres composed mostly of heavier molecules. Since the relative depth of spectral features in a planet’s transmission spectrum results in a direct determination of the atmospheric scale height, the mean molecular weight of that atmosphere can then be calculated by a simple relation (see Eq. 10). For the case of Gl 581c, a hydrogen-rich atmosphere with its large scale height reveals spectral lines in transmission at a level of 10^{-4} . On the other hand, the transmission features for a hydrogen-poor atmosphere will be more than an order of magnitude smaller at a level of less than 10^{-5} . The presence of clouds will not alter this conclusion unless they are unrealistically high in the atmosphere - at a height approaching 10 scale heights above the planet’s surface, where the atmospheric density has dropped off to a point that is difficult to imagine the presence of an optically thick cloud deck. We therefore emphasize that transmission spectroscopy should be a robust method for determining the atmospheric scale height.

The emission spectrum should also be generally helpful in constraining atmospheric hydrogen content. However interpretation can be more complicated than for transmission spectra due to the dependence of the emission spectrum on the atmospheric temperature gradient. For a hydrogen-dominated super-Earth, the emission spectrum should be marked mostly by water features. As we then transition in the cases that we have presented, from H-rich to H-poor, we find that the planetary emission starts showing weaker H_2O features, while absorption due to CO_2 increases. Additionally, the presence of methane or ammonia features for hydrogen-containing atmospheres could be an interesting indication of the photochemistry at work, since these molecules are thought to be destroyed by photodissociation over the lifetime of the planet. Even a weak detection of these features could therefore be helpful in constraining models for atmospheric evolution.

The exact mass of Gl 581c’s atmosphere, which has been chosen somewhat arbitrarily in this paper, has little effect on our spectra presented above. This is due to the simple fact that regions beyond an optical depth of unity are essentially hidden from observers. Therefore, as long as the atmosphere becomes optically thick at some height above the planetary surface, a more massive atmosphere would reveal the same emission and transmission spectra as a less massive one barring any secondary effects such as differing cloud structures. Pressure and temperature conditions near the planetary surface, which would be indicative of the atmospheric mass cannot be observed via spectroscopy for an optically thick atmosphere. For this reason it will be difficult to constrain atmospheric mass with spectral observations. Another negative consequence is that the question of habitability will remain unanswered as long as the planet’s surface conditions are unknown and unobservable. Mass-radius measurements may provide the first constraints on atmospheric mass for super-Earths, however there are large degeneracies in the models that will be difficult to overcome (Adams et al. 2008).

Our simple model for the super-Earth atmosphere has allowed us to understand some of the important effects of hydrogen content on transmission and emission spectra. However, future more

detailed models will be needed to address some of the issues that we have simplified here. A T-P profile that is coupled with a photochemical model is needed to correctly predict some of the feedback mechanisms that occur as photochemistry alters the atmospheric composition. Surface processes also much be considered as they can further affect atmospheric composition through cycles (such as the carbonate-silicate cycle), outgassing, or interactions with a liquid ocean. Additional questions to be addressed by a general super-Earth model are those that plague all planetary atmosphere models such as the presence of clouds and a proper treatment of condensation.

Currently, no transiting super-Earths have been detected. However, CoRoT (Baglin 2003; Barge et al. 2005) and Kepler (Borucki et al. 2004; Basri et al. 2005) missions are both designed with the capability of detecting transiting super-Earths orbiting Sun-like stars. Depending on occurrence rates, a large number of such planets could be discovered in the next 5 years by both of these space-based missions. Additionally, ground-based transit surveys such as MEarth (Nutzman & Charbonneau 2007), which will specifically target M-dwarfs, as well as radial velocity surveys both have the capabilities to detect planets in the super-Earth range. Most interestingly, the combination of these searches should allow for super-Earths to be found in a wide range of orbits and around a variety of types of stars.

Spitzer is currently the only telescope that has demonstrated the capability of observing exoplanet emission and transmission spectra in the mid-IR. Unfortunately, it is unlikely that Spitzer will be able to make the same types of observations for super-Earths, with the possible exception of a warm planet with a hydrogen-rich atmosphere – see Figure 4. Otherwise, measurements would need to be taken at a level of several to tens of ppm. The James Webb Space Telescope (JWST) (Gardner et al. 2006) should fare better, since it has been designed to make these types of measurements at the precision needed. With its expected instrument complement that will allow for narrow band photometry and low to medium resolution IR spectroscopy, JWST should allow for follow-up observations to characterize the atmospheres of transiting Super-Earths. Valenti et al. (in prep.) have simulated JWST NIRSpec spectra for transiting Earth-like planets orbiting M-stars, using atmospheric models from Ehrenreich et al. (2006). They determine that 10 transits (for a 1.4 hr transit duration) and 28 hours of observing time are needed to detect water absorption features in transmission at a $4\text{-}\sigma$ detection threshold. Scaling these values to the hydrogen-rich case for Gl 581c results in a 20-hour integration time and 6 transits needed to detect its transmission features with their expected depth of 10^{-4} . Others have suggested that JWST can do better by up to a factor of two (Swain 2008, submitted). If this is the case, then even less observing time will be needed. These types of observations should be feasible with proper telescope scheduling and should allow for the full richness of super-Earth atmospheres of different sizes, compositions, and orbits to be explored.

We would like to thank Richard Freedman for providing some of the molecular line data for this work, Jonathan Fortney for useful discussion, and our anonymous referee for comments that have helped to improve this paper.

REFERENCES

- Adams, E. R., Seager, S., & Elkins-Tanton, L. 2008, *ApJ*, 673, 1160
- Baglin, A. 2003, *Advances in Space Research*, 31, 345
- Baraffe, I., Selsis, F., Chabrier, G., Barman, T. S., Allard, F., Hauschildt, P. H., & Lammer, H. 2004, *A&A*, 419, L13
- Barge, P., Baglin, A., Auvergne, M., Buey, J.-T., Catala, C., Michel, E., Weiss, W. W., Deleuil, M., Jorda, L., Moutou, C., & COROT Team. 2005, in *SF2A-2005: Semaine de l’Astrophysique Francaise*, ed. F. Casoli, T. Contini, J. M. Hameury, & L. Pagani, 193–+
- Basri, G., Borucki, W. J., & Koch, D. 2005, *New Astronomy Review*, 49, 478
- Beaulieu, J.-P., Bennett, D. P., Fouque, P., Williams, A., Dominik, M., Jorgensen, U. G., Kubas, D., Cassan, A., Coutures, C., Greenhill, J., Hill, K., Menzies, J., Sackett, P. D., Albrow, M., Brilliant, S., Caldwell, J. A. R., Calitz, J. J., Cook, K. H., Cornales, E., & et al. 2006, *Nature*, 439, 437
- Beaulieu, J. P., Carey, S., Ribas, I., & Tinetti, G. 2008, *ApJ*, 677, 1343
- Beichman, C. A., Bryden, G., Gautier, T. N., Stapelfeldt, K. R., Werner, M. W., Misselt, K., Rieke, G., Stansberry, J., & Trilling, D. 2005, *ApJ*, 626, 1061
- Beust, H., Bonfils, X., Delfosse, X., & Udry, S. 2007, *ArXiv e-prints*, 712
- Borucki, W., Koch, D., Boss, A., Dunham, E., Dupree, A., Geary, J., Gilliland, R., Howell, S., Jenkins, J., Kondo, Y., Latham, D., Lissauer, J., & Reitsema, H. 2004, in *ESA SP-538: Stellar Structure and Habitable Planet Finding*, ed. F. Favata, S. Aigrain, & A. Wilson, 177–182
- Brodbeck, C., Nguyen, V.-T., Bouanich, J.-P., Boulet, C., Jean-Louis, A., Bezard, B., & de Bergh, C. 1991, *J. Geophys. Res.*, 96, 17497
- Buccino, A. P., Lemarchand, G. A., & Mauas, P. J. D. 2007, *Icarus*, 192, 582
- Charbonneau, D., Allen, L. E., Megeath, S. T., Torres, G., Alonso, R., Brown, T. M., Gilliland, R. L., Latham, D. W., Mandushev, G., O’Donovan, F. T., & Sozzetti, A. 2005, *ApJ*, 626, 523
- Charbonneau, D., Brown, T. M., Noyes, R. W., & Gilliland, R. L. 2002, *ApJ*, 568, 377
- Charbonneau, D., Knutson, H. A., Barman, T., Allen, L. E., Mayor, M., Megeath, S. T., Queloz, D., & Udry, S. 2008, *ArXiv e-prints*, 802
- Chase, M. W. 1998, *NIST-JANAF Thermochemical Tables* (4th ed.; Washington DC; Am. Chem. Soc.)

- Chevallier, L., Pelkowski, J., & Rutily, B. 2007, *Journal of Quantitative Spectroscopy and Radiative Transfer*, 104, 357
- Chylek, P. & Perez, M. R. 2007, *ArXiv e-prints*, 709
- Deming, D., Harrington, J., Laughlin, G., Seager, S., Navarro, S. B., Bowman, W. C., & Horning, K. 2007, *ApJ*, 667, L199
- Deming, D., Harrington, J., Seager, S., & Richardson, L. J. 2006, *ApJ*, 644, 560
- Deming, D., Seager, S., Richardson, L. J., & Harrington, J. 2005, *Nature*, 434, 740
- Demory, B.-O., Gillon, M., Barman, T., Bonfils, X., Mayor, M., Mazeh, T., Queloz, D., Udry, S., Bouchy, F., Delfosse, X., Forveille, T., Mallmann, F., Pepe, F., & Perrier, C. 2007, *A&A*, 475, 1125
- Ehrenreich, D., Lecavelier des Etangs, A., Hébrard, G., Désert, J.-M., Vidal-Madjar, A., McConnell, J. C., Parkinson, C. D., & Ballester, G. E. 2008, *ArXiv e-prints*, 803
- Ehrenreich, D., Tinetti, G., Lecavelier Des Etangs, A., Vidal-Madjar, A., & Selsis, F. 2006, *A&A*, 448, 379
- Elkins-Tanton, L. & Seager, S. 2008, *ApJ*, submitted
- Fortney, J. J., Marley, M. S., & Barnes, J. W. 2007, *ApJ*, 659, 1661
- Freedman, R. S., Marley, M. S., & Lodders, K. 2007, *ArXiv e-prints*, 706
- Gardner, J. P., Mather, J. C., Clampin, M., Doyon, R., Greenhouse, M. A., Hammel, H. B., Hutchings, J. B., Jakobsen, P., Lilly, S. J., Long, K. S., Lunine, J. I., McCaughrean, M. J., Mountain, M., Nella, J., Rieke, G. H., Rieke, M. J., Rix, H. W., Smith, E. P., Sonneborn, G., Stiavelli, M., Stockman, H. S., Windhorst, R. A., & Wright, G. S. 2006, *Space Science Reviews*, 123, 485
- Grillmair, C. J., Charbonneau, D., Burrows, A., Armus, L., Stauffer, J., Meadows, V., van Cleve, J., & Levine, D. 2007, *ArXiv Astrophysics e-prints*
- Hanel, R. A., Conrath, B. J., Kunde, V. G., Prabhakara, C., Revah, I., Salomonson, V. V., & Wolford, G. 1972, *J. Geophys. Res.*, 77, 2639
- Hansen, B. M. S. 2007, *ApJS*, submitted
- Harrington, J., Luszcz, S., Seager, S., Deming, D., & Richardson, L. J. 2007, *Nature*, 447, 691
- Hubbard, W. B., Hattori, M. F., Burrows, A., Hubeny, I., & Sudarsky, D. 2007, *Icarus*, 187, 358
- Hunten, D. M., Donahue, T. M., Walker, J. C. G., & Kasting, J. F. 1989, *Escape of atmospheres and loss of water (Origin and Evolution of Planetary and Satellite Atmospheres)*, 386–422

- Irvine, W. M., Schloerb, F. P., Crovisier, J., Fegley, Jr., B., & Mumma, M. J. 2000, *Protostars and Planets IV*, 1159
- Knutson, H. A., Charbonneau, D., Allen, L. E., Burrows, A., & Megeath, S. T. 2008, *ApJ*, 673, 526
- Lovis, C., Mayor, M., Pepe, F., Alibert, Y., Benz, W., Bouchy, F., Correia, A. C. M., Laskar, J., Mordasini, C., Queloz, D., Santos, N. C., Udry, S., Bertaux, J.-L., & Sivan, J.-P. 2006, *Nature*, 441, 305
- Massie, S. T. & Hunten, D. M. 1981, *J. Geophys. Res.*, 86, 9859
- Moroz, V. I., Linkin, V. M., Matsygorin, I. A., Spaenkuch, D., & Doehler, W. 1986, *Appl. Opt.*, 25, 1710
- Nutzman, P. & Charbonneau, D. 2007, *ArXiv e-prints*, 709, 345
- Partridge, H. & Schwenke, D. W. 1997, *J. Chem. Phys.*, 106, 4618
- Ribas, I., Guinan, E. F., Güdel, M., & Audard, M. 2005, *ApJ*, 622, 680
- Richardson, L. J., Deming, D., Horning, K., Seager, S., & Harrington, J. 2007, *ArXiv Astrophysics e-prints*
- Rivera, E. J., Lissauer, J. J., Butler, R. P., Marcy, G. W., Vogt, S. S., Fischer, D. A., Brown, T. M., Laughlin, G., & Henry, G. W. 2005, *ApJ*, 634, 625
- Rothman, L. S., Jacquemart, D., Barbe, A., Benner, D. C., Birk, M., Brown, L. R., Carleer, M. R., Chackerian, C., Chance, K., Coudert, L. H., Dana, V., Devi, V. M., Floud, J.-M., Gamache, R. R., Goldman, A., Hartmann, J.-M., Jucks, K. W., Maki, A. G., Mandin, J.-Y., Massie, S. T., Orphal, J., Perrin, A., Rinsland, C. P., Smith, M. A. H., Tennyson, J., Tolchenov, R. N., Toth, R. A., Vander Auwera, J., Varanasi, P., & Wagner, G. 2005, *Journal of Quantitative Spectroscopy and Radiative Transfer*, 96, 139
- Rowe, J. F., Matthews, J. M., Seager, S., Kuschnig, R., Guenther, D. B., Moffat, A. F. J., Rucinski, S. M., Sasselov, D., Walker, G. A. H., & Weiss, W. W. 2006, *ApJ*, 646, 1241
- Rowe, J. F., Matthews, J. M., Seager, S., Miller-Ricci, E., Sasselov, D., Kuschnig, R., Guenther, D. B., Moffat, A. F. J., Rucinski, S. M., Walker, G. A. H., & Weiss, W. W. 2007, *ArXiv e-prints*, 711
- Seager, S., Deming, D., & Valenti, J. A. 2008, in *Astrophysics in the Next Decade: JWST and Concurrent Facilities*, *Astrophysics and Space Science Library*, Thronson, H. A., Tielens, A., Stiavelli, M., eds., Springer: Dordrecht (2008)., ed. H. A. Thronson, A. Tielens, & M. Stiavelli, *Astrophysics and Space Science Library*
- Seager, S., Kuchner, M., Hier-Majumder, C., & Militzer, B. 2007, *ArXiv e-prints*, 707

- Seager, S., Whitney, B. A., & Sasselov, D. D. 2000, *ApJ*, 540, 504
- Selsis, F., Kasting, J. F., Levrard, B., Paillet, J., Ribas, I., & Delfosse, X. 2007, *A&A*, 476, 1373
- Sharp, C. M. & Huebner, W. F. 1990, *ApJS*, 72, 417
- Sotin, C., Grasset, O., & Mocquet, A. 2007, *Icarus*, 191, 337
- Swain, M. R., Bouwman, J., Akeson, R., Lawler, S., & Beichman, C. 2007, *ArXiv Astrophysics e-prints*
- Swain, M. R., Vasisht, G., & Tinetti, G. 2008, *Nature*, 452, 329
- Tinetti, G., Vidal-Madjar, A., Liang, M.-C., Beaulieu, J.-P., Yung, Y., Carey, S., Barber, R. J., Tennyson, J., Ribas, I., Allard, N., Ballester, G. E., Sing, D. K., & Selsis, F. 2007, *Nature*, 448, 169
- Udry, S., Bonfils, X., Delfosse, X., Forveille, T., Mayor, M., Perrier, C., Bouchy, F., Lovis, C., Pepe, F., Queloz, D., & Bertaux, J. . 2007, *ArXiv e-prints*, 704
- Valencia, D., O’Connell, R. J., & Sasselov, D. 2006, *Icarus*, 181, 545
- Valencia, D., Sasselov, D. D., & O’Connell, R. J. 2007, *ApJ*, 665, 1413
- Vidal-Madjar, A., Désert, J.-M., Lecavelier des Etangs, A., Hébrard, G., Ballester, G. E., Ehrenreich, D., Ferlet, R., McConnell, J. C., Mayor, M., & Parkinson, C. D. 2004, *ApJ*, 604, L69
- Vidal-Madjar, A., Lecavelier des Etangs, A., Désert, J.-M., Ballester, G. E., Ferlet, R., Hébrard, G., & Mayor, M. 2003, *Nature*, 422, 143
- von Bloh, W., Bounama, C., Cuntz, M., & Franck, S. 2007a, *ArXiv e-prints*, 712
- . 2007b, *A&A*, 476, 1365
- Wallace, P. J. & Carmichael, I. S. E. 1994, *American Mineralogist*, 79, 161
- White, W. B., Johnson, S. M., & Dantzig, G. B. 1958, *J. Chem. Phys.*, 28, 751
- Wright, G. S., Bortoletto, F., Bruce, Jr., C. F., van Dishoeck, E. F., Karnik, A. R., Lagage, P.-O., Larson, M. E., Lemke, D., Oloffson, G., Miller, E. A., Henning, T. F. E., Heys, S., Ray, T., Rodriguez, J., Serabyn, E., & Walters, I. 2003, in Presented at the Society of Photo-Optical Instrumentation Engineers (SPIE) Conference, Vol. 4850, *IR Space Telescopes and Instruments*. Edited by John C. Mather . Proceedings of the SPIE, Volume 4850, pp. 493-503 (2003)., ed. J. C. Mather, 493–503
- Yung, Y. L. & Demore, W. B., eds. 1999, *Photochemistry of planetary atmospheres*

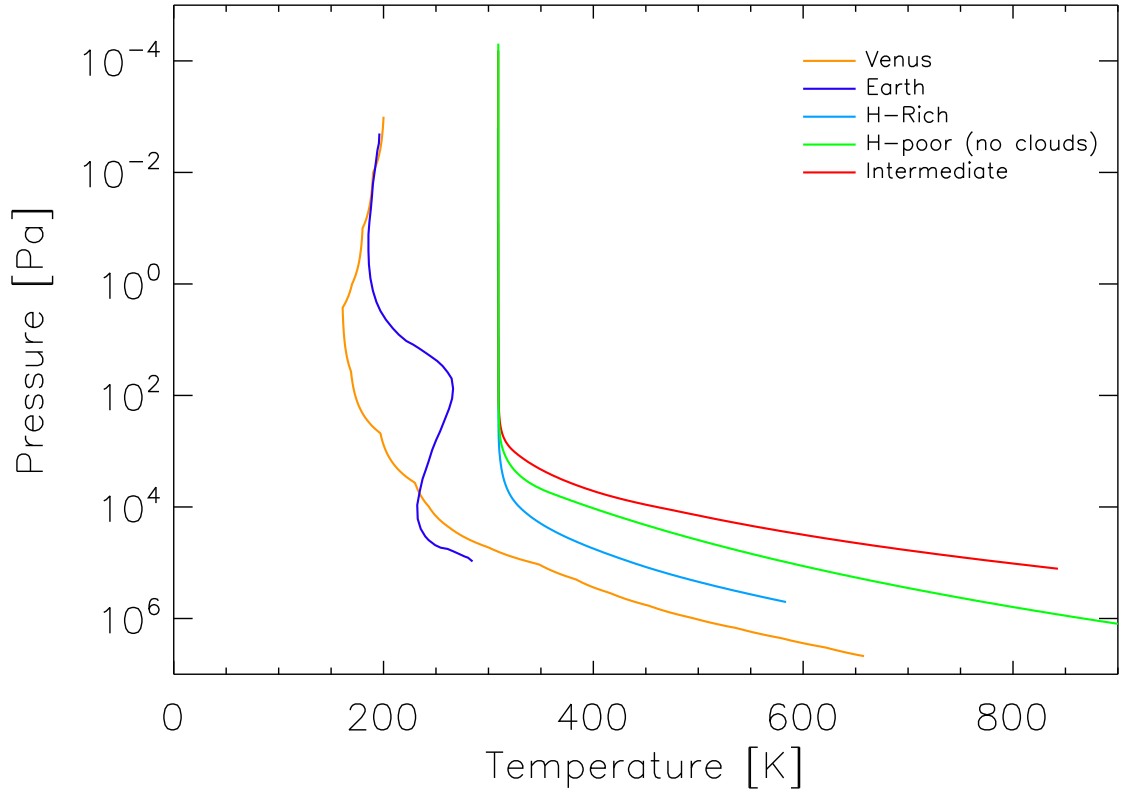


Fig. 1.— Temperature-pressure profiles for each of our three atmosphere scenarios (at $\mu_0 = 0.5$) along with those of Earth and Venus as a reference. Qualitatively, our T-P profiles resemble Venus’, however our model is not capable of reproducing the types of temperature inversions seen in the upper atmospheres of the terrestrial planets.

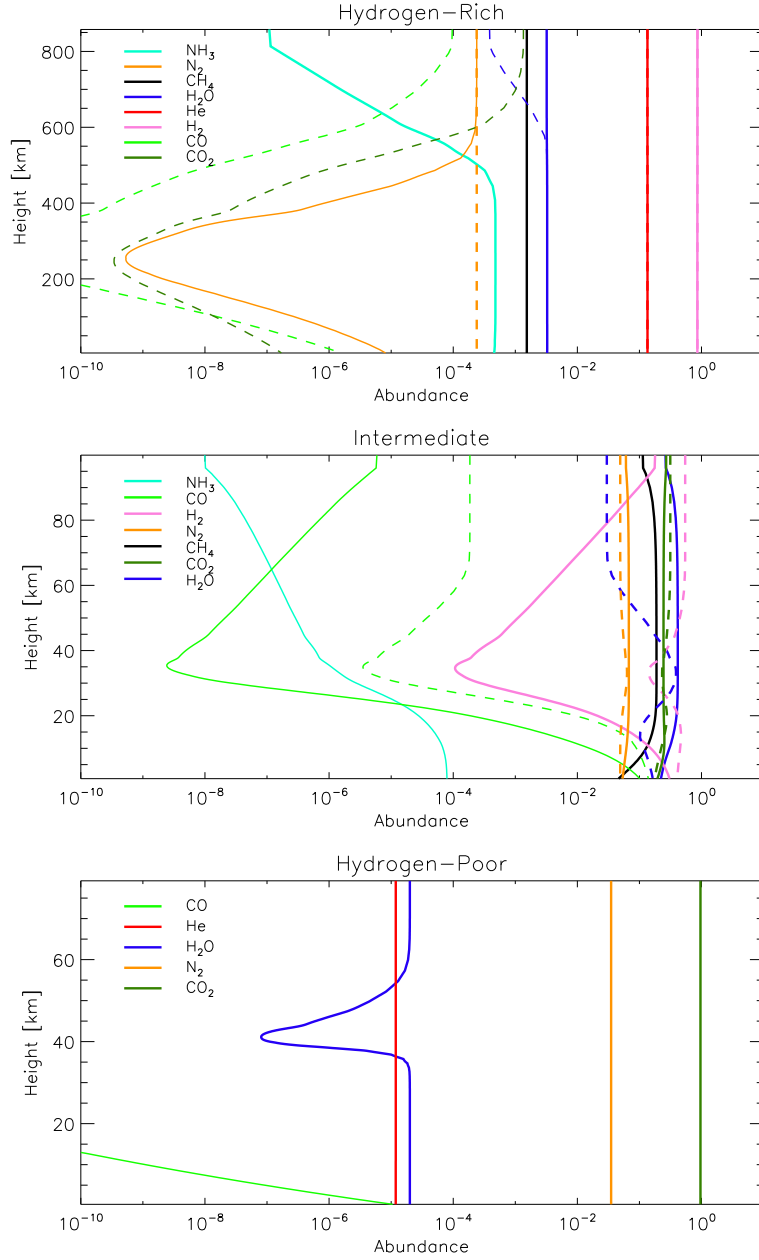


Fig. 2.— Molecular abundances as a function of height for each of the three super-Earth atmosphere scenarios. The solid lines show the results of the chemical equilibrium calculations, while the dashed lines give molecular abundances for the case that NH_3 and CH_4 have been entirely removed from the atmosphere through photodissociation. In the top panel, the solid and dashed lines for both H_2 and He lie essentially on top of one another, since their abundances barely change with the loss of ammonia and methane from the atmosphere.

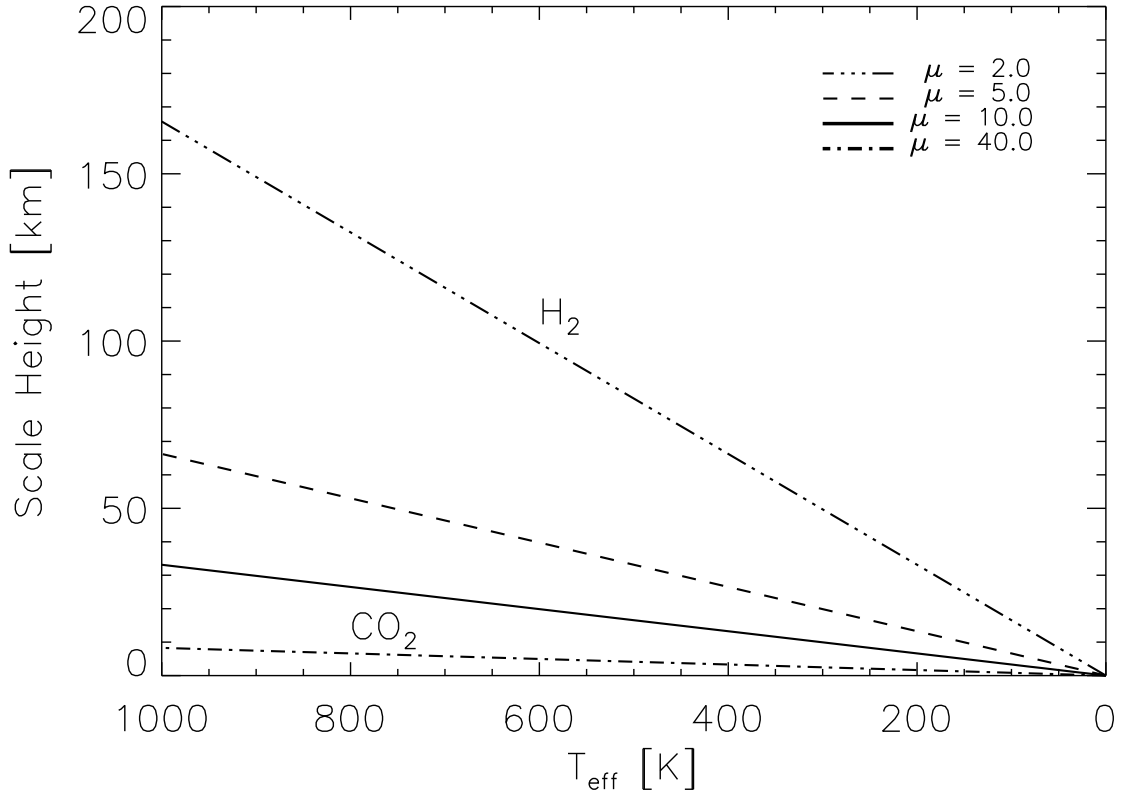


Fig. 3.— Atmospheric scale height as a function of effective temperature for a number of atmospheric compositions. Each line corresponds to a different value of mean molecular weight, μ_m . At the top, $\mu_m = 2$ signifies an atmosphere comprised solely of molecular hydrogen, while the bottom line with $\mu_m = 40$ represents an atmosphere made up of mostly CO_2 . The observability of an exoplanet atmosphere in transmission falls off as molecular weight increases and scale height correspondingly drops off. This plot is for Gl 581c, assuming a surface gravity of 25 m/s^2 .

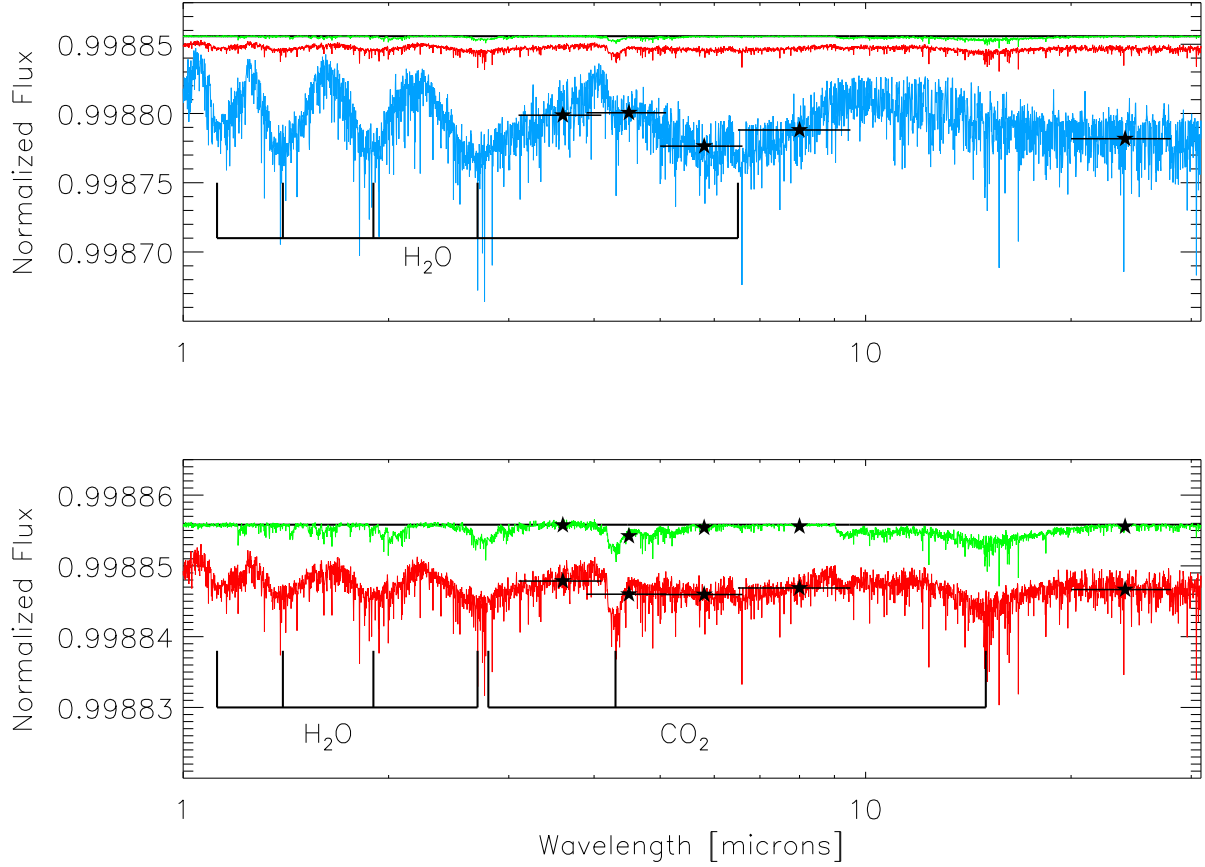


Fig. 4.— Top: Transmission spectra (transit flux divided by out-of-transit flux) of Gl 581c for the cases of a hydrogen-rich atmosphere (blue), an intermediate atmosphere (red), a hydrogen-poor atmosphere (green), and no atmosphere (black line). The stars correspond to the relative flux that would be observed in each of the Spitzer IRAC bands as well as in the 24- μ m MIPS band, and the attached horizontal bars represent the width of each filter. Bottom: Same as above, but zoomed in to show the transmission spectra for the intermediate and hydrogen-poor atmospheres only. Once again, the fluxes expected from the 5 Spitzer bands are overlaid, although the horizontal bars have been omitted in the case of the hydrogen-poor atmosphere so as not to obscure the spectrum.

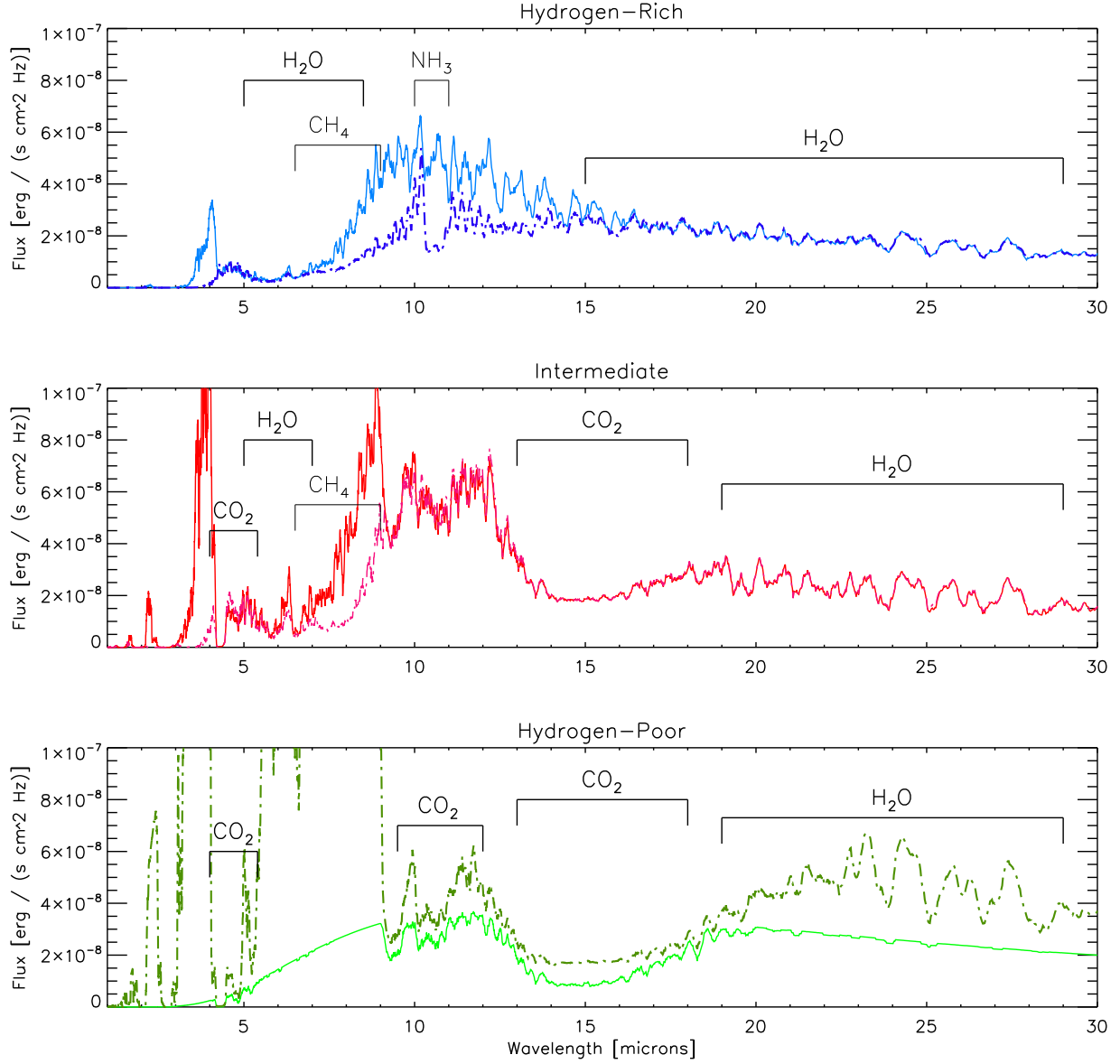


Fig. 5.— Emission spectra of Gl 581c for each of the three cases of atmospheric composition considered in this paper. In the top two panels, the solid lines are the spectra with NH_3 and CH_4 removed due to photochemical considerations. The dashed lines show the same spectra but for an atmosphere in chemical equilibrium. The bottom panel shows the hydrogen-poor emission spectra for a cloud-free model (dashed line) and a model with sulfuric acid clouds at a temperature of 400 K (solid line). The major features have been labeled, including NH_3 and CH_4 features in the dashed-line spectra.

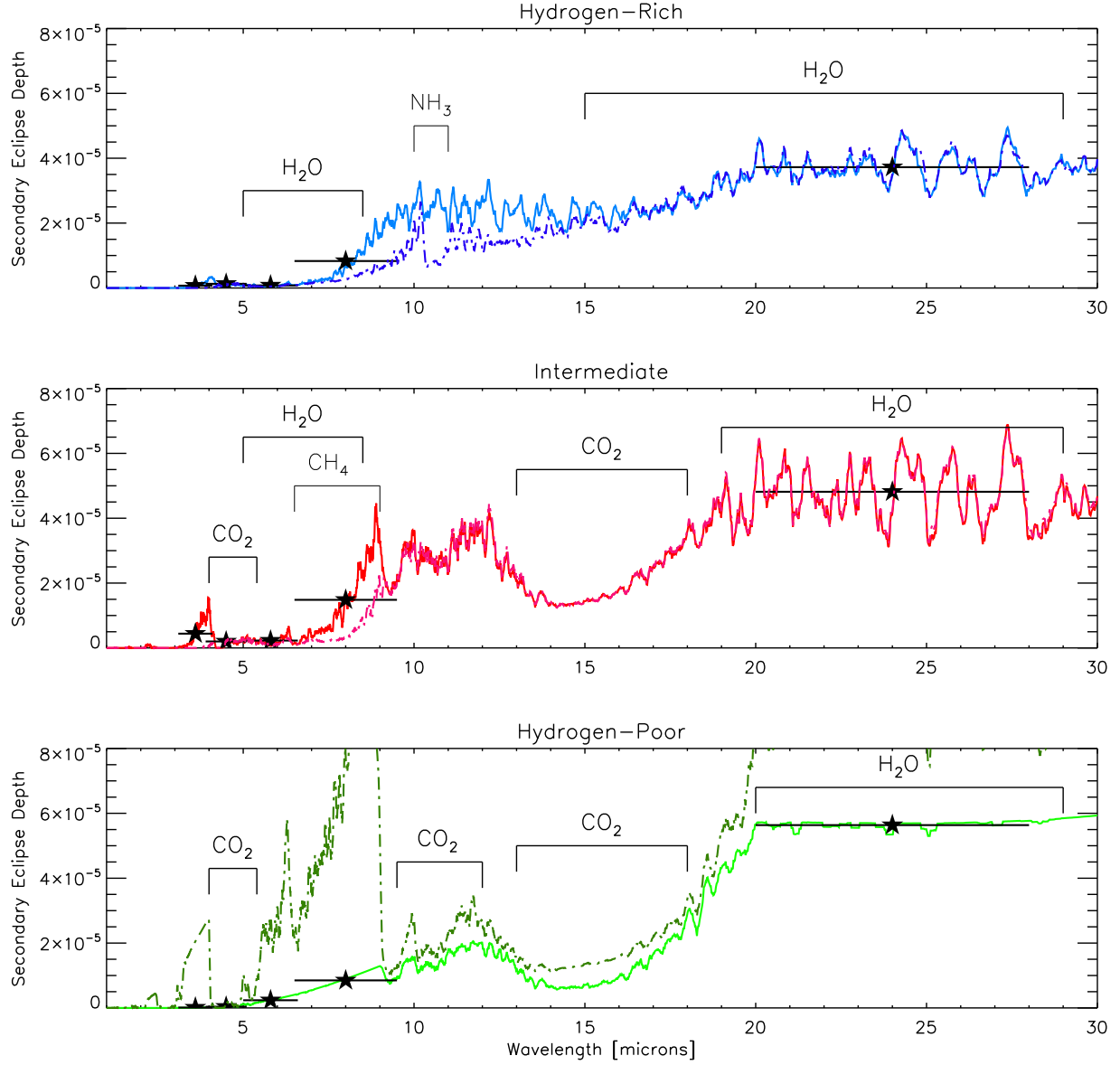


Fig. 6.— Secondary eclipse depths for our three atmosphere scenarios. Dashed lines in the top two panels represent models with methane and ammonia removed due to photochemical considerations. In the bottom panel we include versions of the hydrogen-poor atmosphere both with (solid line) and without (dashed line) sulfuric acid clouds. The major features in the planet’s emission spectrum have been labeled. The model fluxes for the solid-line spectra averaged over the four Spitzer IRAC bands and the 24- μm MIPS band are indicated by stars, and the solid horizontal lines represent the corresponding filter widths.

Table 1. Atomic Composition

Species	H-Rich	Intermediate	H-Poor
H	0.925	0.500	1.4×10^{-5}
He	0.072	trace	4.0×10^{-6}
C	8.2×10^{-4}	0.128	0.325
N	2.6×10^{-4}	0.040	0.024
O	1.9×10^{-3}	0.304	0.651
Ne	1.3×10^{-4}	trace	2.4×10^{-6}
S	2.4×10^{-5}	3.8×10^{-3}	5.1×10^{-5}

Note. — Abundances are all given as mole fractions.